Lignin Compounds to Monoaromatics: Selective Cleavage of C-O Bonds over Brominated Ruthenium Catalyst

Dan Wu, [a,b] Qiyan Wang, [a,b] Olga V. Safonova, [d] Deizi V. Peron, [b] Wenjuan Zhou, [a] Zhen Yan, [a] Maya Marinova, [c] Andrei Y. Khodakov, [b] and Vitaly V. Ordomsky [b]**

[a] *Eco-Efficient Products and Processes Laboratory (E2P2L), UMI 3464 CNRS-Solvay, 201108 Shanghai, People's Republic of China*

[b] *Univ. Lille, CNRS, Centrale Lille, ENSCL, Univ. Artois, UMR 8181 – UCCS – Unité de Catalyse et Chimie du Solide, F-59000 Lille, France, E-mail: vitaly.ordomsky@univ-lille.fr; andrei.khodakov@univ-lille.fr;*

[c] *Univ. Lille, CNRS, INRAE, Centrale Lille, Univ. Artois, FR 2638 - IMEC - Institut Michel-Eugène Chevreul, F-59000 Lille, France*

[d] *Paul Scherrer Institute, 5253 Villigen, Switzerland*

ABSTRACT.

Herein, we propose a heterogeneous Ru/C catalyst modified by Br atoms for the selective direct cleavage of C-O bonds in diphenyl ether without hydrogenation of aromatic rings reaching the yield of benzene and phenol as high as 90.3 %. Characterization of the catalyst indicates selective poisoning by Br of terrace sites over Ru nanoparticles, which are active in the hydrogenation of aromatic rings, while the defect sites on the edges and corners of ruthenium nanoparticles remain available for selective C-O bond cleavage. Moreover, these defect sites exhibit very higher intrinsic activity in the C-O bond cleavage due to the electron withdrawal from Ru by electronegative Br atoms. The elaborated strategy has been applied for depolymerization of lignin. The ruthenium catalysts promoted with bromine exhibited enhanced monomer yield and increased selectivity to mono-aromatics (97.3% vs 46.2%) in comparison with initial Ru.

KEYWORDS. Heterogeneous catalysis; Selective poisoning; Electronic effect; Diphenyl ether; Lignin.

1. Introduction

Renewable energy and chemicals produced from biomass are attracting more and more interest in both academic and industrial communities [1]. Lignocellulose is the most abundant biomass in nature. Hemicellulose and cellulose are formed by hundreds or

thousands sugar units, while lignin is a complex organic polymer constituted from aromatic rings, which are cross-linked via C-C and ether bonds [2]. Production of mono-aromatics from lignin is highly desirable due to the wide application of mono-aromatics as solvents, polymers, dyes, pharmaceuticals etc. [3]. Most of aromatic rings in lignin are linked by phenolic ether bonds, such as β-O-4, α-O-4, and 4-O-5 linkages, in which 4-O-5 is the most stable and robust [4]. Selective cleavage of aryl ether bonds in lignin to produce mono-aromatics is a major challenge in sustainable chemistry.

Due to the complexity and variability of real lignin biomass, diphenyl ether (DPE, 4-O-5 linkages model compound) has been widely used as a lignin model compound for the investigation of the C-O bond cleavage in lignin [5]. Homogeneous molecular catalysts and heterogeneous metal catalysts have been reported for cleavage of aryl ethers [6]. However, homogeneous catalyst suffers from separation problems and high cost. Thus, solid heterogeneous catalyst with high stability and recyclability seem to be a more preferred option for lignin conversion [7].

Numerous heterogeneous catalysts have been reported for the DPE cleavage [4c, 6c], among them, supported metal catalysts appear the most active and selective for this reaction [8]. However, cleavage of aryl ethers over metal catalysts at elevated temperature and high H_2 pressure always causes hydrogenation of aromatic rings in the valuable mono-aromatic products with high consumption of expensive hydrogen [8a, 9]. Specifically, the conversion of DPE over metal catalysts under reductive conditions involves several reaction pathways [6b, 6d, 10]. The first one is direct hydrogenolysis of the C-O bonds with the production of equivalent amounts of phenol (PhOH) and

benzene (Bez). The second path is hydrogenation of the aromatic rings to cyclohexyloxybenzene (CHOBez), cyclohexanol (CHOH), cyclohexane (CHE) and cyclohexyl ether (CHOCH) products. Direct hydrogenolysis of C-O bonds is thermodynamically more favorable than aromatic rings hydrogenation in the first step (-69.62 kJ/mol and -45.44 kJ/mol, respectively). The activation barrier for C-O bonds cleavage is however, very high (314 kJ/mol) [4a, 9c]. This results in mostly kinetic control of the selectivity of the DPE conversion.

Wang et al. have systemically studied the cleavage of C-O bonds in DPE over Ni, Pd, Ru and Pt catalysts [11] and discovered that both hydrogenation of aromatic rings and hydrogenolysis of C-O bonds proceed in parallel. The main products of DPE hydrogenation at high conversion are CHE and CHOH with only trace amounts of monoaromatic products. Hydrogenation of aromatic rings is inevitable during the conversion of DPE. Bimetallic systems have been extensively studied by Zhang et al. [12]. A series of highly efficient Ni-based catalysts have been developed for the hydrogenolysis of lignin to aromatics in the aqueous phase. However, it is still a challenging task to perform selective hydrogenolysis of C-O bonds in 4-O-5 model compounds (e.g., DPE) with the inhibition of aromatic ring hydrogenation.

One of the existing methods for preventing the hydrogenation of aromatic rings is the addition of homogeneous base additives [10b, 13]. Hartwig et al. reported a strategy for the hydrogenolysis of aryl ethers using homogenous and heterogeneous nickel catalysts in the presence of NaO*t*Bu as a base additive [6d, 10b]. Bez and PhOH were produced from DPE without further hydrogenation under mild reaction conditions. However, the

use of base additives suffers from the separation, purification problems and waste utilization. Thus, there is still a challenge for selective cleavage of C-O bonds in DPE without hydrogenation of the aromatic rings.

Hydrogenolysis and hydrogenation happen simultaneously during the catalytic conversion of DPE over metal nanoparticles [6a, 8a, 9c]. These two reactions take place over different active sites. Hydrogenolysis of C-O bonds is favored on the edge and corner sites [14], while hydrogenation of aromatic rings proceeds over the continuous sites on the terrace (**Figure 1**) [1b, 14b, 15]. In order to prevent the hydrogenation of aromatic rings, selective poisoning of the terrace sites could be considered as a possible strategy [16]. Simon et al. reported that furfural transformation could be directed by control of the availability of specific active sites over Pd nanoparticles by selective poisoning with organic thiols [16b]. Bulk organic ligands restrict the adsorption of furfural on terrace sites, while edge and corner sites have been less affected. Although the selectivity of furfural conversion could be tuned by this strategy, the strong poisoning with sulfur caused the loss of activity of the Pd catalysts. Therefore, up to now, selective poisoning of specific active sites on metal nanoparticles without loss of activity is still a challenge.

According to our previous work, supported Pd catalysts modified by iodine and bromine exhibited extremely selective reductive etherification and hydrodeoxygenation of biomass-derived furan compounds [17]. The hydrogenation of aromatic rings has been significantly suppressed over Pd-I and Pd-Br catalysts. Those preliminary results have allowed us putting forward a Ru-Br catalyst for selective catalytic conversion of DPE

under H_2 with high selectivity to mono-aromatic products (Bez and PhOH) and enhanced activity for the C-O bonds cleavage. Characterizations and model reactions indicate that both selective poisoning and electronic effects contribute to the enhanced performance of the catalyst. The developed Ru-Br catalyst is highly efficient for the production of PhOH and Bez from DPE with an overall yield of mono-aromatics up to 90.3% under mild conditions (120°C & 5 bar of H_2).

2. Results and discussion

2.1. Catalytic conversion of DPE over Ru/C and Br-Ru/C

First of all, the conversion of DPE has been screened over Pd/C, Pt/C, and Ru/C catalysts at 120 °C and 5 bar of H_2 in methanol as a solvent. Ru is the most active catalyst in comparison with Pd and Pt for the cleavage of C-O bonds in DPE, which is consistent with the literature (**Table 1, Entry 1-3**) [8a, 8b, 18]. At the same time, Ru/C provides the highest selectivity to monomers (79.2%) in comparison with Pd/C (5.8%). In agreement with previous reports [9c], the monomer products over Ru/C are CHE (40.3%), CHOH (38.9%) and CHOCH (19.1%), indicating high hydrogenation ability of Ru/C for aromatic rings (**Figure 1**).

To prevent the hydrogenation of aromatic rings and to increase the selectivity to valuable aromatic products, Ru/C has been pretreated with the halogens such as Cl, Br and I, via the hydrogenolysis of their corresponding halogenated benzene compounds at reductive conditions. Our previous work [17] has reported that modification of Pd

nanoparticles by Br and I could suppress the hydrogenation of aromatic rings. However, after modification with I, the prepared I-Ru/C catalyst was almost inactive in conversion of DPE (0.8%) indicating total poisoning of Ru surface (**Table 1, Entry 6**). Although Cl-Ru/C has higher activity for DPE transformation, the selectivity to Bez and PhOH was still low (8.9 & 9.7%, respectively, **Table 1, Entry 4**). Most interestingly, Br-Ru/C catalyst exhibited a significant promotion effect in comparison with Cl-Ru/C for the Bez and PhOH production (**Table 1, Entry 5**). The selectivity to the monomer products over Br-Ru/C increased from 79.2 to 98% in comparison with parent Ru/C. The main monomer products over Br-Ru/C are Bez (44.7%) and PhOH (45.6%). It means that the presence of Br almost totally suppressed the hydrogenation of aromatic rings. It is worth noting that the conversion of DPE over Br-Ru/C catalyst is still comparable to Ru/C. It has been reported earlier [19] that the strength of the interaction between noble metals and halogens decreases in the row I > Br > Cl due to the covalent nature of this bond and stronger interaction with the more polarizable (larger) halogen atoms. This trend was also recently observed for Pd nanoparticles [Ref. Dan Wu] Thus, the strong effect of Br could be attributed to the intermediate strength of interaction with Ru and selective bromine adsorption on the terrace sites.

It was suspected that pretreatment of Ru/C by bromobenzene could proceed through oxidative addition of bromobenzene with surface Ru atoms by the modification of Ru surface by Br atoms and release of benzene (**Figure S1, SI**) [20]. To investigate the role of Br source in the generation of selective catalyst, Ru/C has been pretreated by various Br sources. First, Ru/C has been pretreated by the $RuBr_3$ salt. The prepared $RuBr_3$-Ru/C

catalyst shows lower conversion than Br-Ru/C and still high selectivity to Bez and PhOH (73.4%, **Table 1, Entry 7**). This indicates that the Ru-Br species on the Ru surface are responsible for the promotion of catalytic performance. Notably, pure $RuBr_3$ salt has no activity for DPE conversion (**Table 1, Entry 8)**. It suggests that both Ru-Br species and metallic Ru are needed for the conversion of DPE to Bez and PhOH. Ru/C catalyst pretreated by HBr has also been prepared (**Table 1, Entry 9**). HBr-Ru/C catalyst shows high DPE conversion (95.2%) but lower mono-aromatics selectivity (39.8%) in comparison with Br-Ru/C. This result indicates that HBr cannot effectively modify the Ru surface most probably because of lower reactivity between HBr and noble metal Ru. It is worth noting that in the presence of the HBr in the reagents, the conversion of DPE significantly decreased over Ru/C, which could be ascribed to the competitive adsorption of HBr with reactants on the catalyst (**Table1, Entry 10**) [17b].

To evaluate the effect of support, Ru nanoparticles supported on SiO_2 and Al_2O_3 have been pretreated by bromobenzene and subjected to hydrogenation of DPE. The parent Ru/SiO_2 and Ru/Al_2O_3 catalysts demonstrate lower conversion of DPE in comparison with Ru/C (**Table 1, Entry 11 & 13**). This decline of activity could be ascribed to the lower metal dispersions in the Ru/SiO_2 and Ru/Al_2O_3 catalysts (**Table S1 & Figure S2, SI**) [21]. It has been reported earlier that hydrogenolysis of C-O bonds is a structure-sensitive reaction [14a, 14b]. The defect sites localized on the edges and corners are responsible for the C-O bond cleavage. The highly dispersed Ru nanoparticles on carbon support have a higher fraction of edge and corner sites than Ru supported over SiO_2 and Al_2O_3 leading to higher catalytic activity (**Table 1, Entry 3, 11 & 13**). The

conversion of DPE decreased from 47.4 on Ru/SiO_2 to 18.6% over $Br\text{-}Ru/SiO_2$, and decreased from 49.3 on Ru/Al_2O_3 to 14.9 % over $Br\text{-}Ru/Al_2O_3$ (**Table 1, Entry 12 & 14**). At the same time, Ru/C demonstrates almost the same activity after Br deposition with total change of the product distribution by suppression of aromatic rings hydrogenation activity (**Table S2, SI**).

The most efficient catalyst for the DPE conversion, Br-Ru/C has been used for further catalytic tests. **Figure 2** shows the evolution of DPE conversion and product selectivity over the Ru/C and Br-Ru/C catalysts in time. Hydrogenation of DPE over the initial Ru/C catalyst yields Bez, PhOH and CHOBez as the main products at the initial time in agreement with the literature [8a, 8b, 18, 22]. However, at longer reaction time, the selectivity to Bez and PhOH continuously decreases and the selectivity to CHE, CHOH, and CHOCH increases. Notably, the selectivity to CHOBez increases from 23.4 to 30.7 % at the beginning of the reaction with a subsequent decrease. This is due to the secondary hydrogenation and hydrogenolysis of CHOBez. The final products over initial Ru/C at high conversions are CHE (40.3%), CHO (38.9%) and CHOCH (19.1%).

Interestingly, the Br-Ru/C catalyst demonstrates a different reaction pathway. The reaction proceeds with the generation of Bez and PhOH as main products reaching the selectivity of 44.7% and 45.6% at high conversion, respectively. The hydrogenation of aromatic rings has been suppressed during the whole reaction time. Notably, the total yield of mono-aromatic products (Bez and PhOH) was 90.3 % over the Br-Ru/C catalyst in comparison to 0% over the initial Ru/C catalyst at full conversion. A small amount of etherification products (< 2%) such as methoxycyclohexane and anisole

were observed over both Ru/C and Br-Ru/C due to the reaction with methanol as a solvent. This reaction requires acid sites. The low selectivity to ether products indicates the absence of acid sites over both Ru/C and Br-Ru/C catalysts [17a]. According to our previous reports, Pd-I and Pd-Br could generate in-situ Brønsted acid sites by heterolytic dissociation of H_2 [17]. However, different to Pd-I and Pd-Br, pyridine (Py)-FTIR studies (**Figure S3, SI**) have demonstrated that no Brønsted acid sites were generated over Ru-Br in the presence of H_2. Thus, hydrogenation of aromatic rings and hydrogenolysis of C-O bonds proceed simultaneously over Ru/C, while mainly hydrogenolysis of C-O bonds takes place over Br-Ru/C. Although the hydrogenation of aromatic rings was suppressed over Br-Ru/C, the DPE conversion over the catalyst did not decrease.

The stability of the Br-Ru/C catalyst has been confirmed by the catalytic test of DPE conversion at 120 °C under 5 bar of H_2 in three consecutive cycles with intermediate separation of the catalyst and products (**Figure 3**). The catalyst demonstrates almost comparable activity in the DPE conversion for 3 cycles (**Figure 3a**). At the same time, the selectivity to Bez and PhOH remained high and close to 50 %, confirming the high stability of the Ru-Br catalyst (**Figure 3b**). The leaching of Br^- in the solution during catalysis has been also checked by the addition of $AgNO_3$ and has shown the absence of Br^- in the solution (**Figure S4, SI**).

In order to provide further insights into the modification of ruthenium catalysts with bromine, we calculated the activity normalized by total number of metal surface sites

(TOF) on the basis of the CO adsorption for total DPE conversion, hydrogenation and hydrogenolysis (**Table 2**).

Table 2 shows that TOF for overall DPE conversion was only very slightly higher for Ru/C compared to the Ru/SiO_2 sample, while TOFs for hydrogenation and hydrogenolysis were very different. Indeed, smaller Ru nanoparticles on carbon exhibit a higher hydrogenolysis TOF, since they contain a higher fraction of defect sites such as corners and edges, while larger nanoparticles with a larger fraction of terrace sites over silica show higher TOF in the hydrogenation of aromatics.

The bromine deposition on both carbon and silica supported ruthenium catalysts results on the one hand, in a dramatic decrease in TOF for the DPE hydrogenation, which is probably due to selective steric blocking of the terrace sites. On the other hand, TOF for hydrogenolysis has increased after the bromine deposition. The enhancement of hydrogenolysis after the modification with bromine is an interplay of electronic and steric effects. The hydrogenolysis seems to take place over defects sites such as corners and edges of the ruthenium nanoparticles. These sites remain available for the reaction after the bromine deposition, though their intrinsic activity has changed. Both CO-FTIR and XPS show electron withdrawal from Ru metal sites in carbon and silica supported catalysts by the bromine species and generation of positively charged Ru nanoparticles. While the steric effect due to the selective blocking of Ru terraces sites is responsible for the drop of the DPE hydrogenation rate, the electronic effects arising from the electron transfer from Ru to the bromine species could explain an increase in intrinsic

activity of Ru surface sites for the hydrogenolysis of the electron-rich C-O bonds on both carbon and silica-supported catalysts (**Table 2**)."

2.2. Characterization

The role of Br in the modification of the catalytic performance of Ru has been studied using different characterization tools. First of all, the Ru-Br catalyst was subjected to STEM-EDS analysis to determine the localization of Br. Obviously, the Br signal has the same position as Ru, confirming that the pretreatment with bromobenzene leads to the preferential localization of the Br atoms over the Ru nanoparticles (**Figure 4**).

The amount of Br in the Ru-Br catalyst supported on C and SiO_2 were analyzed by XRF analysis (**Table 3**). An obvious correlation has been observed between metal dispersion, measured by the CO adsorption and amount of Br. According to the CO-chemisorption, the average particle size of Ru in Ru/SiO_2 is around 15.6 nm with Ru dispersion of 6.7 % in comparison with 1.9 nm nanoparticles with dispersion of 45 % in Ru/C (**Table 3**). At the same time, Br-Ru/C contains 1.0 wt. % of Br and $Br\text{-}Ru/SiO_2$ contains 0.23 wt. % of Br. Moreover, the elemental analysis for the used Br-Ru/C and $Br\text{-}Ru/SiO_2$ catalysts demonstrated no loss of Br, confirming the stability of Ru-Br catalyst (**Table S3, SI**). Notably, taking into account the amount of Br and surface Ru atoms, the ratio of Br to the Ru surface atoms is 56% on Br-Ru/C and 88% on $Br\text{-}Ru/SiO_2$. Higher Br coverage over $Br\text{-}Ru/SiO_2$ suggests that most of Ru surface sites are occupied by the Br atoms. The Br adsorption therefore, can occur on the terrace sites of the Ru nanoparticles.

FTIR spectroscopy of CO adsorption has been used further to confirm the localization of Br (**Figure 5**). The Ru/SiO_2 catalyst has the band at 1998 cm^{-1} assigned to CO linearly adsorbed on the defect sites of edges and corners of Ru nanoparticle [16d]. The intensive band at 1877 cm^{-1} is related to CO adsorption on the multiple terrace Ru sites [23]. The modification of Ru by Br leads to the complete disappearance of the peak at 1877 cm^{-1}. At the same time, the linear bonded CO peak shifts to a higher frequency from 1998 to 2006 cm^{-1}. The disappearance of the multiple-bonded CO could be explained by the selective deposition of Br atoms on the Ru nanoparticle terraces. The blue shift of the peak related to CO adsorption on edges and corners could be explained by the withdrawal of electrons from Ru to Br with the generation of the positively charged Ru nanoparticles [24]. Moreover, an additional small peak at 2072 cm^{-1} could be assigned to the CO adsorption on the Ru-Br species with highly electron-deficient Ru sites [17b, 25]. Thus, FTIR spectroscopy confirms our earlier assumptions about selective poisoning of terrace sites of Ru nanoparticles by Br.

XPS analysis was carried out to determine the electronic state of Br and Ru in the Br-Ru/C catalyst. **Figure 6** shows the Ru 3p and Br 3d spectra of Br-Ru/C catalyst before and after reaction in comparison with the spectra of initial Ru/C. The Ru 3p spectrum displays 3p3/2 and 3p1/2 components with 22.2 eV spin-orbit splitting [26]. As shown in **Figure 6a**, initial Ru/C has a major peak with BE (Ru 3p3/2) at 461.6 eV attributed to metallic Ru^0 with a small contribution of oxidized Ru^{4+} (RuO_2) [27]. A minor shift of Ru 3p peaks of metallic Ru to higher BE for Br-Ru/C catalysts (both before and after reaction) can be attributed to the interaction of Ru with Br and electron withdrawal

effect from Ru to Br [28]. Interestingly, a new Ru species with BE at 462.5 eV was detected in Br-Ru/C (both before and after reaction) similar to $RuBr_3$ (463.0 eV) and can be assigned to the Ru-Br species.

Br 3d spectra of the considered Ru-Br samples are shown in **Figure 6b**, demonstrating 3d5/2 and 3d3/2 spin-orbit doublets with 1.04 eV splitting [29]. The Br-Ru/C catalyst (both before and after reaction) has the Br 3d5/2 peak with BE=68.3 eV, which is lower in comparison with Br ions in $RuBr_3$ at 68.5 eV. It indicates the more negatively charging Br species in Ru-Br catalyst in comparison with $RuBr_3$. It is worth noting that Br-Ru/C after reaction shows similar Ru 3p and Br 3d spectra suggesting high stability of the Ru-Br catalyst.

Thus, XPS also indicates the electronic withdrawal of electrons from Ru to Br. It has been reported that the electronic properties of metal nanoparticles can affect their reactivity towards different functional groups [30]. For example, the negatively charged Pd nanoparticles modified with phosphine ligands show higher affinity for electronic deficiency molecules such as nitrobenzene but lower affinity for electronic rich groups such as benzyl aldehydes, comparing with the non-modified counterparts [30a].

The localization and coordination state of Br on Ru nanoparticles was further checked by synchrotron-based extended X-ray adsorption fine structure spectroscopy (EXAFS) and X-ray adsorption near-edge structure spectroscopy (XANES). The K absorption-edge of Ru in Br-Ru/C (both before and after reaction) shifts toward higher energy compared with the initial Ru/C catalyst (**Figure 7a**). This phenomenon further reveals that the Ru atoms in Br-Ru/C get more positively charged than that in initial Ru/C

confirming the electronic withdrawal from Ru to Br. The Ru K-edge EXAFS spectra fits of Br-Ru/C exhibit mainly Ru-Ru bonds characteristic for metal nanoparticles and significant the presence of Ru-Br bonding (**Figure 7b & Figure S5, Table S4, SI**). This can be related to a smaller fraction of Ru-Br bonds in comparison to Ru-Ru in Br-Ru/C. This is due to a 5 times higher concentration of Ru, weaker scattering from Br in comparison to Ru and a large disorder in Ru-Br bonds presenting on the surface. Br K-edge EXAFS clearly indicates only Br-Ru in the local structure of Br in Br-Ru/C, confirming the modification of Ru surface by Br atoms (**Figure 7 c & d**).

It is worth noting that the coordination state of Br in Ru-Br catalyst is different in comparison with $RuBr_3$. As it is indicated in **Figure 7c & d**, the XANES and EXAFS of Br K-edges show different features for Br-Ru/C and $RuBr_3$. According to Br K edge EXAFS fit (**Figure S6 & Table S5, SI**) the Br-Ru bonds in Ru-Br/C catalyst are by ca. 0.05 Å longer in comparison with those bonds in $RuBr_3$, which could be explained by Br localization over Ru nanoparticle. The selective coordination of Br on the terraces contributes to the suppression of aromatic rings hydrogenation in DPE conversion. Moreover, the Br-Ru/C catalyst after reaction shows quite similar spectra to fresh one, suggesting the high stability of Ru-Br bonds.

According to the characterization, we can conclude that the modification of Ru nanoparticles with bromobenzene leads to the selective deposition of Br atoms on the terrace sites of Ru nanoparticles with an electronic withdraw from Ru to Br. Selective poisoning of the Ru terrace sites with Br suppresses aromatic ring hydrogenation with the efficient production of mono-aromatic products from DPE.

2.3. Model reactions

To support these conclusions, additional model reactions have been performed over the Ru/C and Br-Ru/C catalysts. These model experiments include hydrogenation of Bez, biphenyl, PhOH and hydrogenolysis of benzyl alcohol. These model reactions aim to demonstrate different activity patterns of the Ru/C and Br-Ru/C catalysts in aromatic ring hydrogenation and C-O bonds hydrogenolysis. **Figure 8** shows higher activity of Ru/C catalyst for hydrogenation of aromatic rings in Bez, PhOH and biphenyl molecules, compared to the Br-Ru/C catalyst. It confirms that the selective poisoning of Ru nanoparticles with Br has dramatically suppressed the hydrogenation of aromatic rings. At the same time, a higher activity for the C-O bond hydrogenolysis in benzyl alcohol to toluene has been observed over the Br-Ru/C catalyst. Thus, the model reactions confirm that the high selectivity to Bez and PhOH in DPE conversion over Ru-Br catalyst derives from the suppression of aromatic rings hydrogenation and enhancement of C-O bonds hydrogenolysis. This promotion effect can be assigned to the synergy of selective poisoning of the terrace sites by Br and electron withdrawal from Ru nanoparticles to Br. Both these phenomena make the Br-Ru/C catalyst outstanding for mono-aromatic production from DPE in the absence of base additives (**Table S6, SI**).

2.4. Conversion of Lignin over Ru-Br catalyst

Furthermore, real lignin has been used as a substrate to confirm the higher activity and selectivity of the Br-Ru/C catalyst for the C-O bond hydrogenolysis. The cleavage of

lignin has been performed at 180 °C under 5 bar of H_2 pressure. These are relatively mild conditions in comparison with the literature (**Table S7, SI**). As it is shown in **Figure 9**, no reaction takes place without a catalyst. In the presence of the catalyst, mostly seven monomers were detected in the reaction mixture (**Figure 9**). The product yield and selectivity to these seven monomer products have been calculated by using cyclohexanol as an internal standard. The yield of monomers over initial Ru/C is 11.6 wt.% with the selectivity to mono-aromatics of 46.1 wt.%. The main product of the reaction is cyclohexane (53.5 wt.%) due to the higher rate of aromatic ring hydrogenation over non-promoted Ru. Surprisingly, Br-Ru/C shows significantly higher yield of monomers (26.2 wt.%) in comparison with Ru/C with the selectivity to the mono-aromatic products reaching 97.3 wt.%. The high activity and higher selectivity to monoaromatic monomer of Br-Ru/C confirms our finding that the positively charged Ru nanoparticles have higher activity for the C-O bonds cleavage. Higher selectivity to mono-aromatic products demonstrates that indeed, selective poisoning of Ru nanoparticles by Br effectively suppresses the aromatic ring hydrogenation. The enhanced productivity of mono-aromatics from lignin opens perspectives for industrial applications of the ruthenium catalysts promoted with bromine for selective deoxygenation of numerous oxygenates (**Table S7, SI**).

3. Conclusion

In this work, the Ru catalysts promoted with bromine were developed for selective deoxygenation reactions. The Ru-Br catalysts exhibited higher activity and selectivity

for cleavage of diphenyl ether to benzene and phenol. Characterization using a combination of methods has provided insights into the modification of the catalyst structure after the promotion with bromine. First, we found that the Br atoms were selectively deposited on the terrace sites preventing the aromatic rings hydrogenation. The cleavage of the C-O bond occurs on corner and edge surface sites over Ru nanoparticles. Second, the electronic withdrawal from Ru to Br results in positive charging of the bared-Ru sites on edges and corners. The positively charged Ru exhibits higher activity for the hydrogenolysis of electron-rich C-O bonds. The elaborated strategy has been applied for selective production of monoaromatic monomers from lignin under mild reactions conditions. Numerous perspectives for selective deoxygenation of various oxygenates, including complex organic polymers have been unveiled.

AUTHOR INFORMATION

Corresponding Author

Andrei Khodakov: E-mail: andrei.khodakov@univ-lille.fr;

Vitaly Ordormsky: E-mail: vitaly.ordomsky@univ-lille.fr;

Unité de Catalyse et de Chimie du Solide

UMR 8181 CNRS, Ecole Centrale de Lille, Université de Lille

Bât. C3, 59655 Villeneuve d'Ascq, France

Author Contributions

The manuscript was written through contributions of all authors. All authors have given approval to the final version of the manuscript.

ASSOCIATED CONTENT

Supporting Information: GC and GC-MS images; XRD and TEM images; Py-FTIR; Summary of characterizations; Literature analysis.

ACKNOWLEDGEMENTS

The authors thank Solvay and University of Lille for stipend for the PhD research of D.W. and financial support of this work. The authors thank the Chevreul Institute (FR 2638) for its help in the development of this work. Chevreul Institute and the Microscopy Platform in Lille is supported by the « Ministère de l'Enseignement Supérieur et de la Recherche et de l'Innovation», the « CNRS » the « Région Hauts-de-France », the « Métropole Européenne de Lille » and the « Fonds Européen de Développement des Régions ». The Swiss Light Source synchrotron is acknowledged for the use of beam time.

Reference

[1] a) R. Gerardy, D. P. Debecker, J. Estager, P. Luis, J. M. Monbaliu, *Chem. Rev.* **2020**, *120*, 7219-7347; b) C. Mondelli, G. Gozaydin, N. Yan, J. Perez-Ramirez, *Chem. Soc. Rev.* **2020**, *49*, 3764-3782; c) X. Wu, N. Luo, S. Xie, H. Zhang, Q. Zhang, F. Wang, Y. Wang, *Chem. Soc. Rev.* **2020**, *49*, 6198-6223.

[2] a) F. Gao, J. D. Webb, H. Sorek, D. E. Wemmer, J. F. Hartwig, *ACS Catal.* **2016**, *6*, 7385-7392; b) S. Gazi, *Appl. Catal. B* **2019**, *257,* 117936; c) C. W. Lahive, P. J. Deuss, C. S. Lancefield, Z. Sun, D. B. Cordes, C. M. Young, F. Tran, A. M. Slawin, J. G. de Vries, P. C. Kamer, N. J. Westwood, K. Barta, *J. Am. Chem. Soc.* **2016**, *138*, 8900-8911.

[3] a) J. Lin, X. Wu, S. Xie, L. Chen, Q. Zhang, W. Deng, Y. Wang, *ChemSusChem* **2019**, *12*, 5023-5031; b) C. Zhou, J. Shi, W. Zhou, K. Cheng, Q. Zhang, J. Kang, Y. Wang, *ACS Catal.* **2019**, *10*, 302-310; c) S. S. Wong, R. Shu, J. Zhang, H. Liu, N. Yan, *Chem. Soc. Rev.* **2020**, *49*, 5510-5560; d) J. Zhang, J. Sun, Y. Wang, *Green Chem.* **2020**, *22*, 1072-1098.

[4] a) J. He, C. Zhao, J. A. Lercher, *J. Am. Chem. Soc.* **2012**, *134*, 20768-20775; b) S. T. Nguyen, P. R. D. Murray, R. R. Knowles, *ACS Catal.* **2019**, *10*, 800-805; c) Z. Sun, B. Fridrich, A. de Santi, S. Elangovan, K. Barta, *Chem. Rev.* **2018**, *118*, 614-678.

[5] a) F. Mauriello, E. Paone, R. Pietropaolo, A. M. Balu, R. Luque, *ACS Sustain. Chem. Eng.* **2018**, *6*, 9269-9276; b) M. Oregui-Bengoechea, I. Agirre, A. Iriondo, A. Lopez-Urionabarrenechea, J. M. Requies, I. Agirrezabal-Telleria, K. Bizkarra, V. L. Barrio, J. F. Cambra, *Top. Curr. Chem.* **2019**, *377*, 36; c) G.-Y. Xu, J.-H. Guo, Y.-C. Qu, Y. Zhang, Y. Fu, Q.-X. Guo, *Green Chem.* **2016**, *18*, 5510-5517.

[6] a) L. Jiang, H. Guo, C. Li, P. Zhou, Z. Zhang, *Chem. Sci.* **2019**, *10*, 4458-4468; b) H. Li, G. Song, *ACS Catal.* **2019**, *9*, 4054-4064; c) V. Patil, S. Adhikari, P. Cross, H. Jahromi, *Renew. Sust. Energ. Rev.* **2020**, *133,* 110359; d) A. G. Sergeev, J. F. Hartwig, *Science* **2011**, *332*, 439-443.

[7] a) M. Gale, C. M. Cai, K. L. Gilliard-Abdul-Aziz, *ChemSusChem* **2020**, *13*, 1947-1966; b) S. Rautiainen, D. Di Francesco, S. N. Katea, G. Westin, D. N. Tungasmita, J. S. M. Samec, *ChemSusChem* **2019**, *12*, 404-408.

[8] a) M. Guo, J. Peng, Q. Yang, C. Li, *ACS Catal.* **2018**, *8*, 11174-11183; b) M. Hua, J. Song, C. Xie, H. Wu, Y. Hu, X. Huang, B. Han, *Green Chem.* **2019**, *21*, 5073-5079; c) M. Wang, H. Shi, D. M. Camaioni, J. A. Lercher, *Angew. Chem. Int. Ed.* **2017**, *56*, 2110-2114.

[9] a) L. Zhang, Y. Wang, L. Zhang, Z. Chi, Y. Yang, Z. Zhang, B. Zhang, J. Lin, S. Wan, *Ind. Eng. Chem. Res.* **2020**, *59*, 17357-17364; b) G. Yao, G. Wu, W. Dai, N. Guan, L. Li, *Fuel* **2015**, *150*, 175-183; c) S. Bulut, S. Siankevich, A. P. van Muyden, D. T. L. Alexander, G. Savoglidis, J. Zhang, V. Hatzimanikatis, N. Yan, P. J. Dyson, *Chem. Sci.* **2018**, *9*, 5530-5535.

[10] a) W. Zhao, X. Li, H. Li, X. Zheng, H. Ma, J. Long, X. Li, *ACS Sustain. Chem. Eng.* **2019**, *7*, 19750-19760; b) A. G. Sergeev, J. D. Webb, J. F. Hartwig, *J. Am. Chem. Soc.* **2012**, *134*, 20226-20229.

[11] a) M. Wang, O. Y. Gutierrez, D. M. Camaioni, J. A. Lercher, *Angew. Chem. Int. Ed.* **2018**, *57*, 3747-3751; b) M. Wang, H. Shi, D. M. Camaioni, J. A. Lercher, *Angew. Chem. Int. Ed.* **2017**, *56,* 2110-2114; c) M. Wang, Y. Zhao, D. Mei, R. M. Bullock, O. Y. Gutiérrez, D. M. Camaioni, J. A. Lercher, *Angew. Chem. Int. Ed.* **2020**, *59*, 1445-1449.

[12] a) J. Zhang, H. Asakura, J. van Rijn, J. Yang, P. Duchesne, B. Zhang, X. Chen, P. Zhang, M. Saeys, N. Yan, *Green Chem.* **2014**, *16*, 2432-2437; b) J. Zhang, J. Teo, X. Chen, H. Asakura, T. Tanaka, K. Teramura, N. Yan, *ACS Catal.* **2014**, *4*, 1574-1583.

[13] F. Gao, J. D. Webb, J. F. Hartwig, *Angew. Chem. Int. Ed.* **2016**, *55*, 1474-1478.

[14] a) L. Dong, L.-L. Yin, Q. Xia, X. Liu, X.-Q. Gong, Y. Wang, *Catal. Sci. Technol.* **2018**, *8*, 735-745; b) F. Yang, D. Liu, Y. Zhao, H. Wang, J. Han, Q. Ge, X. Zhu, *ACS Catal.* **2018**, *8*, 1672-1682; c) L. Zhang, M. Zhou, A. Wang, T. Zhang, *Chem. Rev.* **2020**, *120*, 683-733; d) C. C. Chiu, A. Genest, A. Borgna, N. Rosch, *Phys. Chem. Chem. Phys.* **2015**, *17*, 15324-15330.

[15] a) V. V. Pushkarev, K. An, S. Alayoglu, S. K. Beaumont, G. A. Somorjai, *J. Catal.* **2012**, *292*, 64-72; b) G. Chacón, J. Dupont, *ChemCatChem* **2018**, *11*, 333-341.

[16] a) B. Legras, V. V. Ordomsky, C. Dujardin, M. Virginie, A. Y. Khodakov, *ACS Catal.* **2014**, *4*, 2785-2791; b) S. H. Pang, C. A. Schoenbaum, D. K. Schwartz, J. W. Medlin, *Nat. Commun.* **2013**, *4*, 2448; c) D. J. M. Snelders, N. Yan, W. Gan, G. Laurenczy, P. J. Dyson, *ACS Catal.* **2012**, *2*, 201-207; d) F. Zhang, J. Fang, L. Huang, W. Sun, Z. Lin, Z. Shi, X. Kang, S. Chen, *ACS Catal.* **2018**, *9*, 98-104.

[17] a) D. Wu, W. Y. Hernández, S. Zhang, E. I. Vovk, X. Zhou, Y. Yang, A. Y. Khodakov, V. V. Ordomsky, *ACS Catal.* **2019**, *9*, 2940-2948; b) D. Wu, S. Zhang, W. Y. Hernández, W. Baaziz, O. Ersen, M. Marinova, A. Y. Khodakov, V. V. Ordomsky, *ACS Catal.* **2021**,*11*, 19-30.

[18] a) H. Wu, J. Song, C. Xie, C. Wu, C. Chen, B. Han, *ACS Sustain. Chem. Eng.* **2018**, *6*, 2872-2877; b) L. Zhang, Y. Wang, Y. Yang, B. Zhang, S. Wang, J. Lin, S. Wan, Y. Wang, *Catal. Today* **2020**.

[19] T. Roman, F. Gossenberger, K. Forster-Tonigold, A. Gross, *Phys. Chem. Chem. Phys.* **2014**, *16*, 13630-13634.

[20] H. Weissman, X. Song, D. Milstein, *J. Am. Chem. Soc.* **2001**, *123*, 337-338.

[21] S. Cao, J. R. Monnier, C. T. Williams, W. Diao, J. R. Regalbuto, *J. Catal.* **2015**, *326*, 69-81.

[22] Z. Luo, Z. Zheng, Y. Wang, G. Sun, H. Jiang, C. Zhao, *Green Chem.* **2016**, *18*, 5845-5858.

[23] S. Campisi, D. Ferri, A. Villa, W. Wang, D. Wang, O. Kröcher, L. Prati, *J. Phys. Chem. C* **2016**, *120*, 14027-14033.

[24] S. Xu, S. Chansai, Y. Shao, S. Xu, Y.-c. Wang, S. Haigh, Y. Mu, Y. Jiao, C. E. Stere, H. Chen, X. Fan, C. Hardacre, *Appl. Catal. B* **2020**, *268*, 118752.

[25] J. Wojciechowska, M. Jedrzejczyk, J. Grams, N. Keller, A. M. Ruppert, *ChemSusChem* **2019**, *12*, 639-650.

[26] L. M. Martínez-Prieto, M. Puche, C. Cerezo-Navarrete, B. Chaudret, *J. Catal.* **2019**, *377*, 429-437.

[27] J. Zhao, W. Y. Hernández, W. Zhou, Y. Yang, E. I. Vovk, M. Capron, V. Ordomsky, *ChemCatChem* **2019**, *12*, 238-247.

[28] G. Liang, Y. Zhou, J. Zhao, A. Y. Khodakov, V. V. Ordomsky, *ACS Catal.* **2018**, *8*, 11226-11234.

[29] L. Smykalla, P. Shukrynau, M. Korb, H. Lang, M. Hietschold, *Nanoscale* **2015**, *7*, 4234-4241.

[30] a) M. Guo, H. Li, Y. Ren, X. Ren, Q. Yang, C. Li, *ACS Catal.* **2018**, *8*, 6476-6485; b) T. Komanoya, T. Kinemura, Y. Kita, K. Kamata, M. Hara, *J. Am. Chem. Soc.* **2017**, *139*, 11493-11499; c) G. Chen, C. Xu, X. Huang, J. Ye, L. Gu, G. Li, Z. Tang, B. Wu, H. Yang, Z. Zhao, Z. Zhou, G. Fu, N. Zheng, *Nat. Mater.* **2016**, *15*, 564-569.

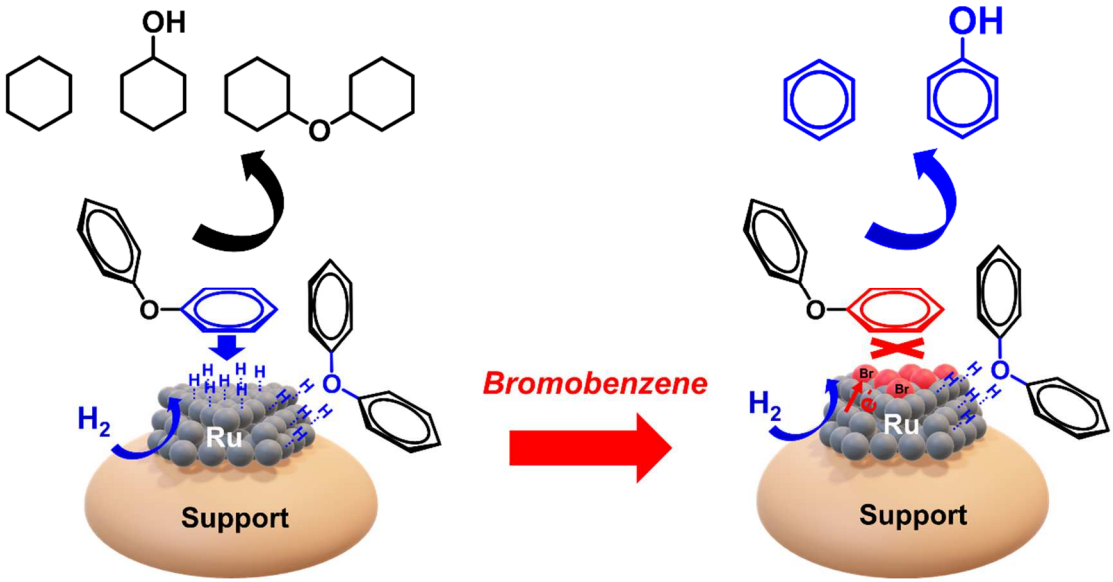

Figure 1. *Illustration of adsorption and conversion of DPE over Ru and Ru-Br catalyst.*

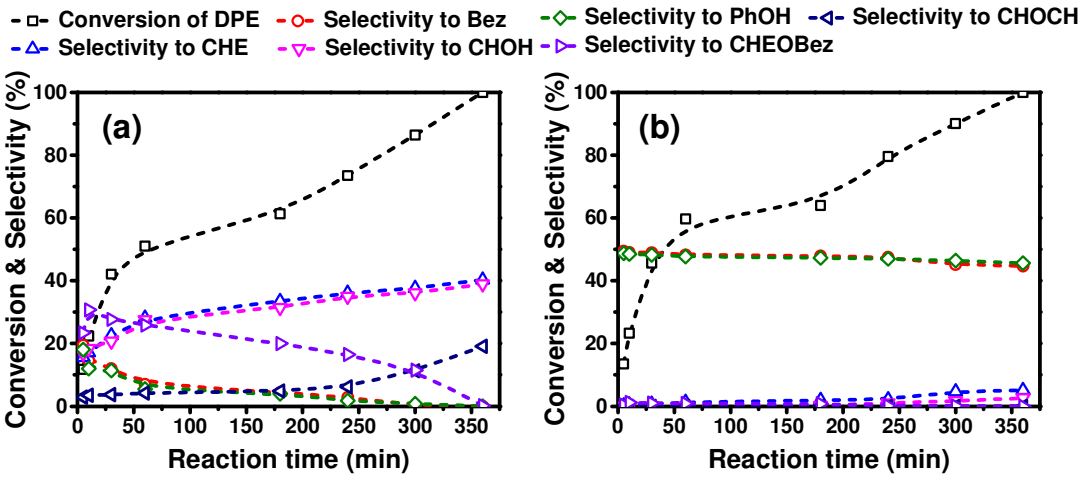

Figure 2. *Evolution of conversion of DPE and selectivity to various products over (a) Ru/C, and (b) Br-Ru/C catalysts. Reaction conditions: 50 mg catalyst, 100 mg DPE, 5 g methanol, 120°C, 5 bar H_2.*

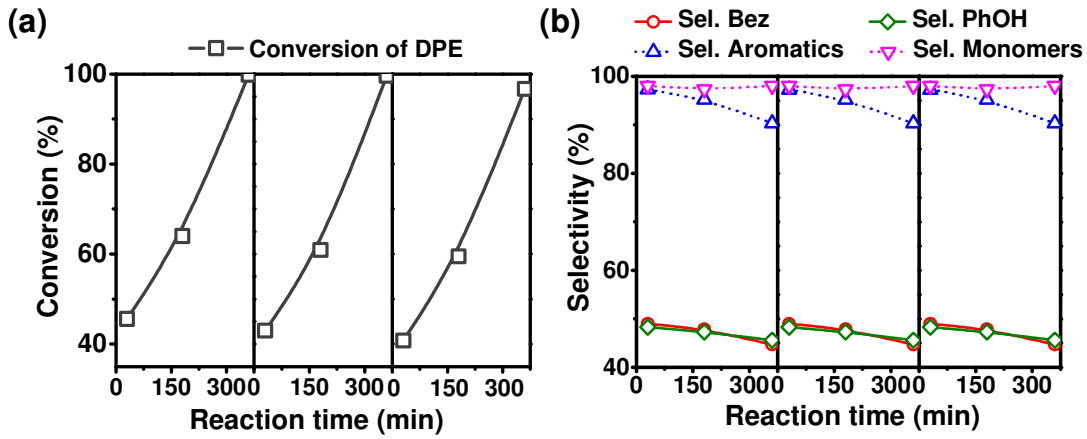

Figure 3. *Stability test of Br-Ru/C catalyst (a) conversion of DPE; (b) selectivity to different products.*

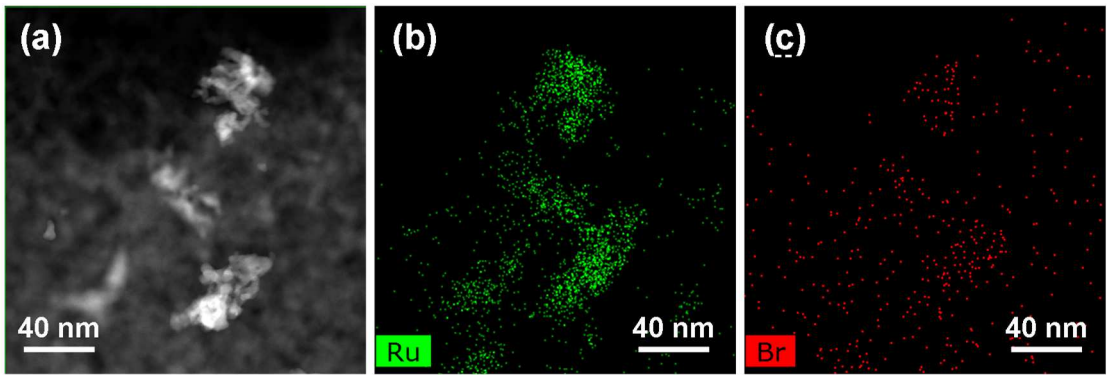

Figure 4. *TEM-EDS analysis (a) STEM image, (b & c) corresponding EDS elemental maps of Br-Ru/SiO_2 catalyst.*

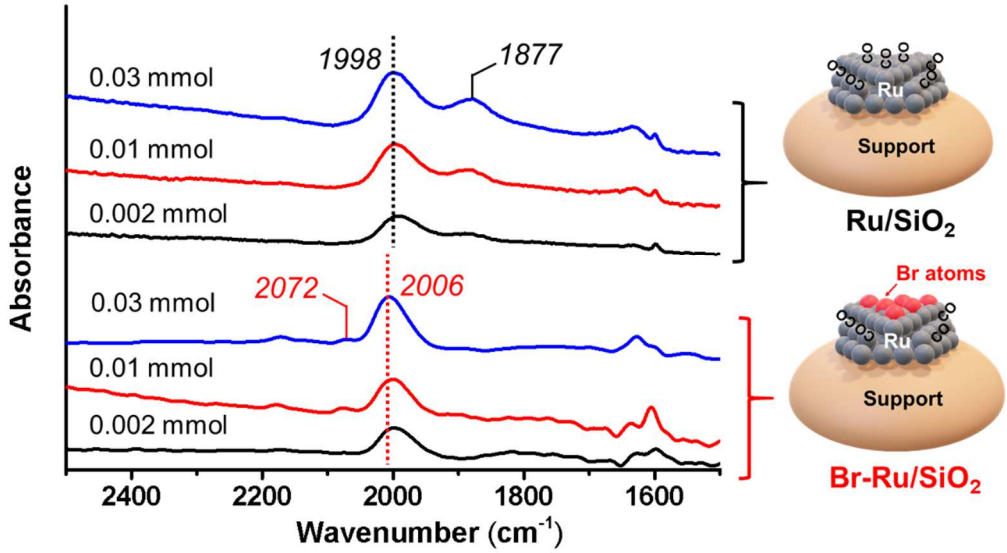

Figure 5. *CO-FTIR for Ru/SiO_2 and Br-Ru/SiO_2*

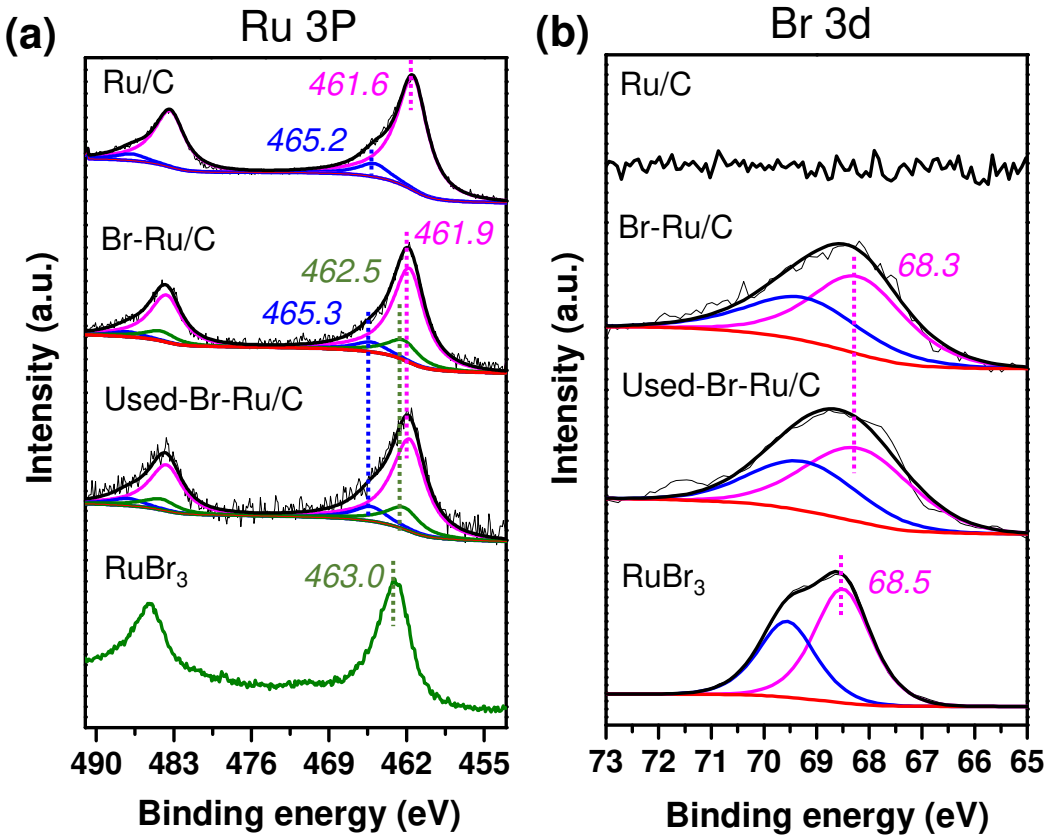

Figure 6. *XPS analysis of (a) Ru 3p and (b) Br 3d core level spectra of Ru/C, Br-Ru/C, Br-Ru/C after reaction and $RuBr_3$ reference.*

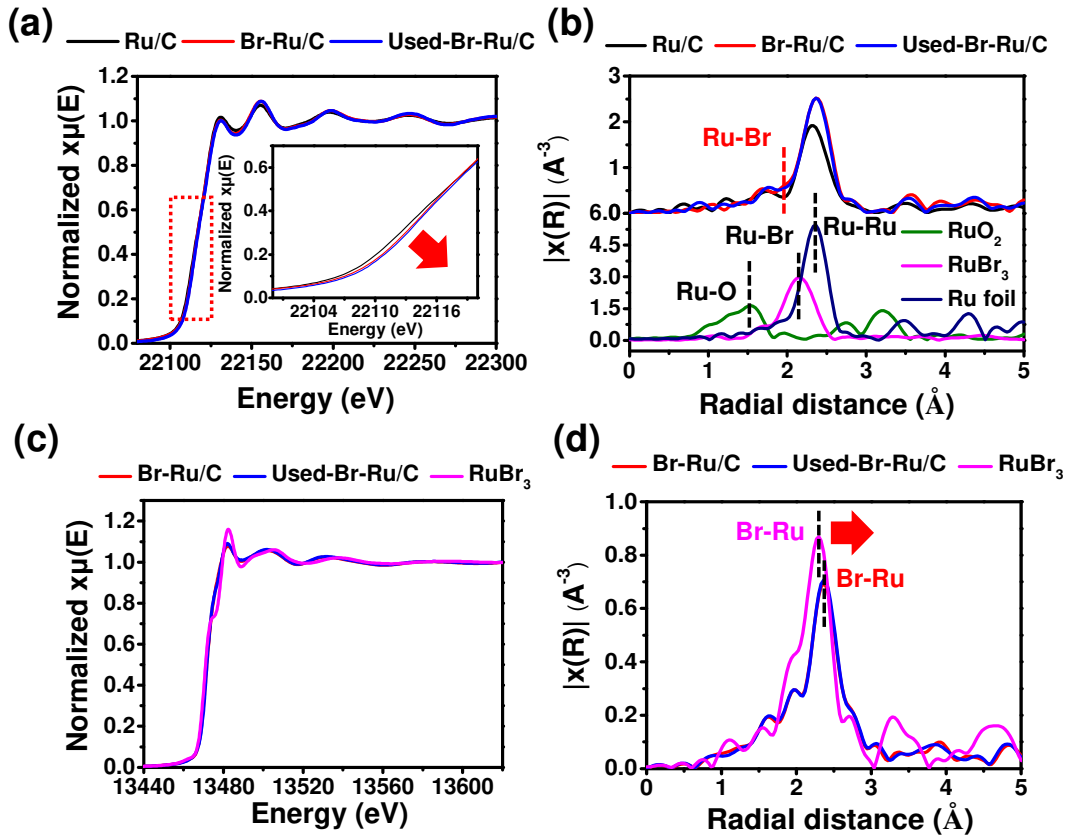

Figure 7. *XANES and EXAFS for (a & b) Ru K-edge and (c & d) Br K-edge.*

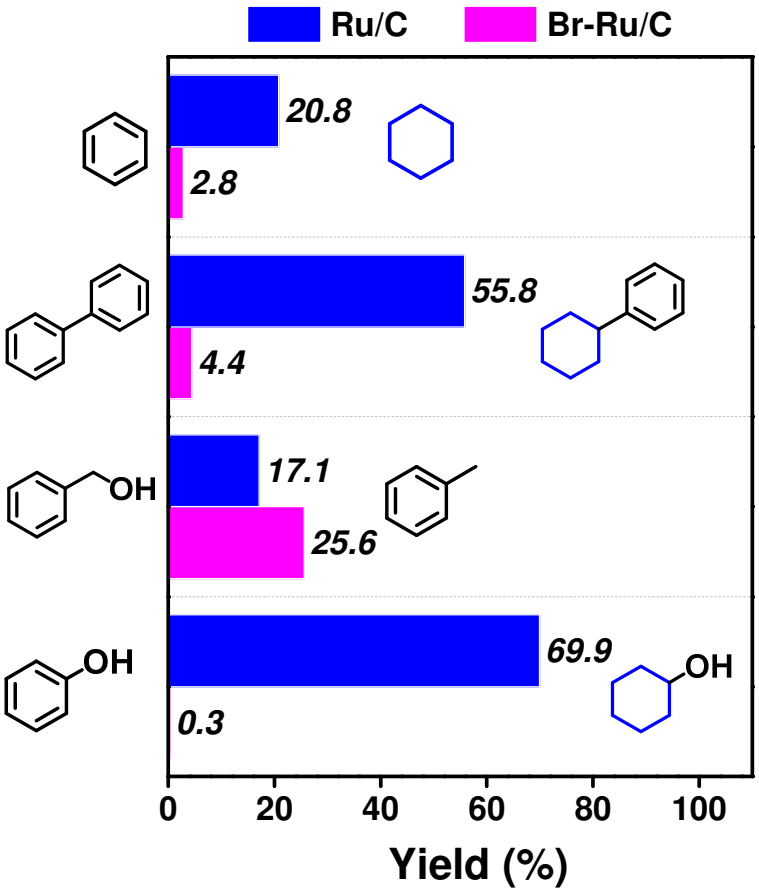

Figure 8. *Model reactions of hydrogenation of Bez, biphenyl, benzyl alcohol, and PhOH over Ru/C and Br-Ru/C catalysts, respectively. Reaction conditions: Benzyl alcohol hydrogenolysis: 15 mg catalyst, 200 mg benzyl alcohol, 5 g methanol, 80°C, 5 bar H_2, 30 min; Biphenyl hydrogenation: 50 mg catalyst, 200 mg biphenyl, 5 g methanol, 120oC, 5 bar H_2, 1 h; Bez hydrogenation: 50 mg catalyst, 200 mg biphenyl, 5 g methanol, 120°C, 5 bar H_2, 1 h; PhOH hydrogenation: 50 mg catalyst, 200 mg benzyl alcohol, 5 g methanol, 80°C, 5 bar H_2, 30 min.*

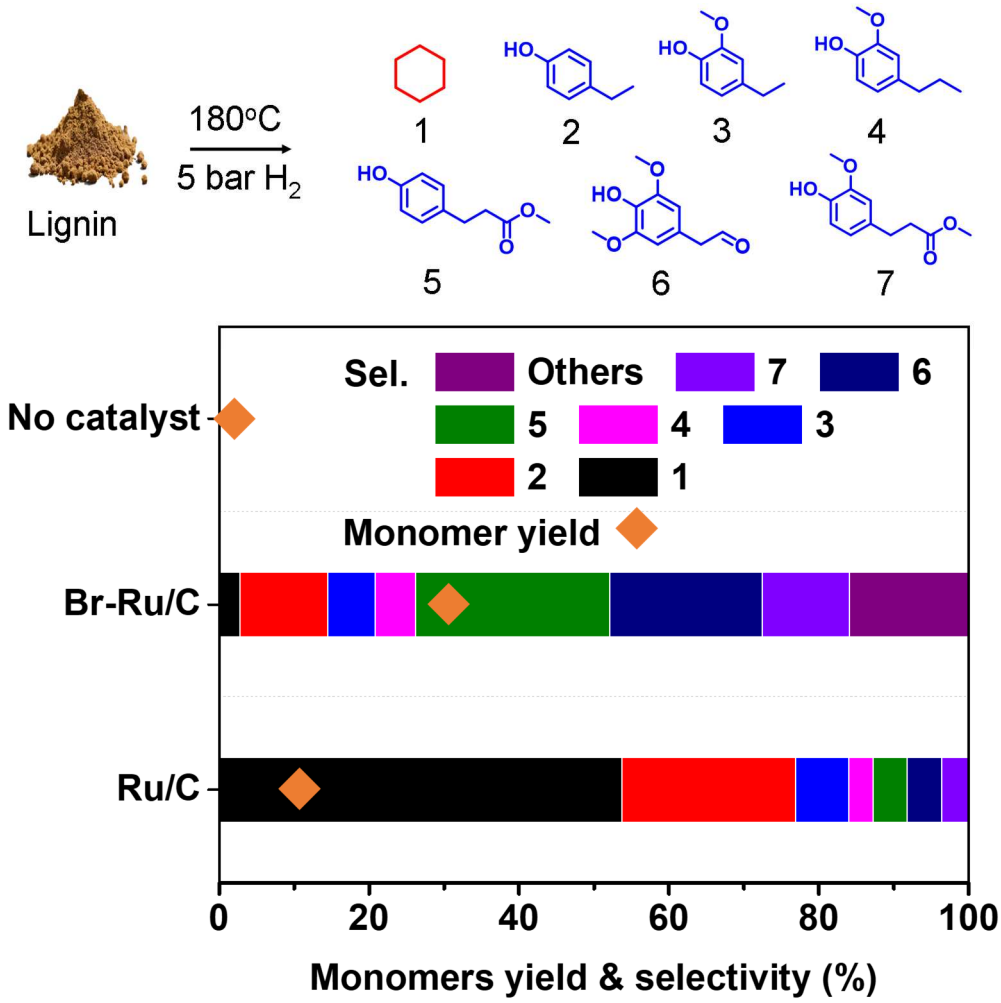

Figure 9. *Conversion of lignin to aromatics over Ru/C and Br-Ru/C catalyst. Reaction conditions: 100 mg of lignin, 100 mg of catalyst, 5 g methanol, 5 bar of H_2, 180°C, 6h.*

Table 1. *Catalytic conversion of DPE over various catalysts. Reaction conditions: 100 mg DPE, 50 mg catalyst, 5 g methanol, 120°C. 5 bar H_2, 6 h.*

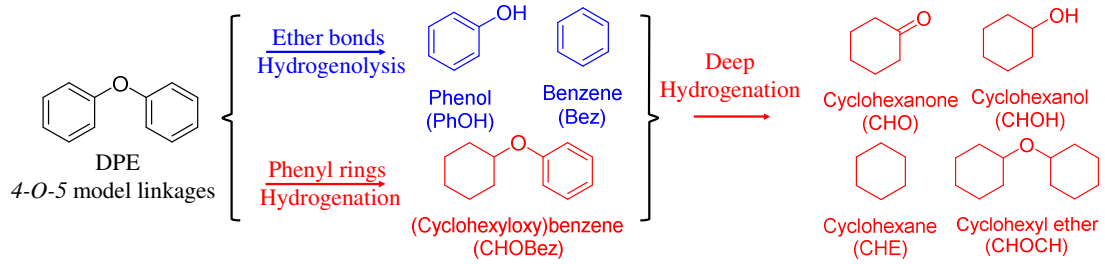

Entry	Cat.	Conv. (%)	Selectivity (%)								
			Bez	CHE	CHOH	PhOH	CHOCH	CHOBez	Oth. [a]	Ar. [b]	Mono. [c]
Screen of metals and halogens											
1	Pd/C	58.4	1.9	1.8	1.7	0.4	5	84.8	4.4	2.3	5.8
2	Pt/C	3.3	0	0	0	0	0	98.8	1.2	0.0	0
3	Ru/C	100	0	40.3	38.9	0	19.1	0.2	1.5	0.0	79.2
4	Cl-Ru/C	100	8.9	35.6	31.9	9.7	12.5	0.4	1	18.6	86.1
5	Br-Ru/C	99.8	44.7	5.1	2.6	45.6	0	0	2	90.3	98
6	I-Ru/C	0.8	-	-	-	-	-	-	-	-	-
7	$RuBr_3$-Ru/C	57.1	27	23.8	1.2	46.4	0	1.5	0.1	73.4	98.4
8	$RuBr_3$	0.5	-	-	-	-	-	-	-	-	-
9	HBr-Ru/C	95.2	21.6	27.2	28.9	18.2	0.5	1.8	1.8	39.8	95.9
10	Ru/C + HBr	26.2	46.3	1.1	0.3	49.2	0	0.2	2.9	95.5	96.9
11	Ru/SiO_2	47.4	5.1	23.5	20.8	4.6	4.2	39.5	2.3	9.7	54
12	Br-Ru/SiO_2	18.6	48.4	1	1.4	47.6	0	0.9	0.7	96.0	98.4
13	Ru/Al_2O_3	49.3	5.1	31.4	36.8	5.9	2	18.8	0	11.0	79.2
14	Br-Ru/Al_2O_3	14.9	34.6	15.2	0	47.4	0	0.9	1.9	82.0	97.2

[a] Other products include ether and acetal products such as methoxycyclohexane, anisole, (dimethoxymethyl)cyclohexane, and (dimethoxymethyl)benzene.

[b] Sum selectivity to mono-aromatics includes benzene and phenol.

[c] Sum selectivity to monomers includes benzene, cyclohexane, phenol, and cyclohexanol.

Table 2. *TOF numbers of DPE over Ru/C and Ru/SiO_2 both before and after Br modification*

Catalyst	Conversion (%) [a]	Metal dispersion [b] (%)	TOF (min^{-1}) [d]		
			DPE	Hydrogenolysis	Hydrogenation
Ru/C	11.8	45	1.24	0.87	0.77
Br-Ru/C	13.8	45	1.42	1.40	0.01
Ru/SiO_2 [e]	14.4	6.7	0.85	0.06	0.94
Br-Ru/SiO_2 [f]	18.6	6.7	0.18	0.18	0.01

[a] Reaction conditions: 100 mg DPE, 50 mg catalyst, 5 g methanol, 120°C. 5 bar H_2, 5 min.

[b] Ru dispersion was determined by CO-chemisorption.

[d] Turnover frequency (TOF) was calculated based on metal dispersion, Br-Ru/C has the same metal dispersion as initial Ru/C.

[e] Reaction conditions: 100 mg DPE, 50 mg Ru/SiO_2, 5 g methanol, 120°C. 5 bar H_2, 60 min.

[f] Reaction conditions: 100 mg DPE, 50 mg Br-Ru/SiO_2, 5 g methanol, 120°C. 5 bar H_2, 360 min.

Table 3. *Summary of the results obtained from the characterizations of Ru and Ru-Br supported on C and SiO_2.*

Catalyst	Element analysis (wt. %) [a]		Br amount (mmol/g)	Surface Ru [b] (mmol/g)	Br Coverage [c] (%)
	Ru	Br			
Ru/C	4.9	0	0	0.223	-
Br-Ru/C	4.9	1.0	0.125	0.223	56
Ru/SiO_2	4.7	0	0	0.033	-
$Br-Ru/SiO_2$	4.7	0.23	0.029	0.033	88

[a] The amount of Br and Ru were determined by XRF analysis, Ru content in Ru/C was provided by the suppliers.

[b] The amount of surface Ru was calculated from the CO-chemisorption, Ru dispersion over Ru/C is 45%, and 6.7% over Ru/SiO_2.

[c] Br coverage was calculated by divided Br amount by surface Ru.

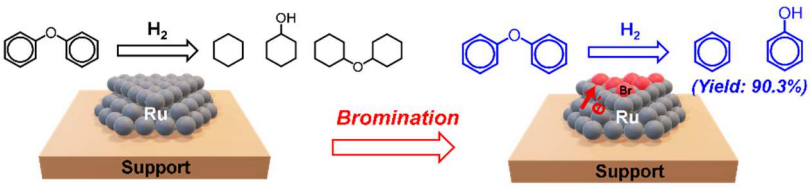

Graphical abstract: A brominated supported Ru catalyst has been developed for the cleavage of C-O linkages in aryl ethers in biomass-derived lignin compounds without hydrogenation of the aromatic rings. Both selective poisoning of terrace sites and electronic promotion of defect sites contribute to the catalytic performance. A high yield reaching 90.3 % to monoaromatics from diphenyl ether have been observed under mild reaction conditions.